Supplementary data

Modulating Surficial Oxygen Vacancy of VO_2 Nanostructure to Boost Its Electromagnetic Absorption Performance

Siyao Cheng,[a,b] Aming Xie,[a,*] Xihao Pan,[b] Kexin Zhang,[a] Cheng Zhang,[b] Xiangpeng Lin,[b] and Wei Dong[b]

[a] School of Mechanical Engineering, Nanjing University of Science and Technology, Nanjing 210094, China

[b] School of Chemical Engineering, Nanjing University of Science and Technology, Nanjing 210094, China

* Corresponding author: xieaming@njust.edu.cn (A. Xie)

1. Experimental section

***Preparation of MoO_3-$B_{0.5}$*:** Prepare commercial MoO_3 (1 g) and $NaBH_4$ (0.5 g) to a mortar, and then grinding the solid mixture using pestle for 20 min until it turns black. Instantaneously, transfer the solids mixture from the mortar into a beaker of cold water. Then stirring for 1 h until no bubbles appear in the solution, indicating that excess $NaBH_4$ has been removed. The final precipitations are collected by vacuum filtration and wash with methanol and distilled water twice times, and then dry in a vacuum at 60℃ for 12 h.

2. Supported table

Table S1. The area of the corresponding individual component is fitted by the peak for VO_2 and VO_2-B_x (x = 0.05, 0.3, 1.0).

	V4+ 2p3/2	V5+ 2p3/2	V4+ 2p1/2	V5+ 2p1/2	O1s	OH
VO_2	11900.622	13599.736	6637.54	6095.68	23375.79	7553.521
VO_2-$B_{0.05}$	14186.112	10787.608	5093.46	5164.53	15501.81	5001.279
VO_2-$B_{0.3}$	11565.824	8233.9145	4206.58	4330.59	27722.54	1130.806
VO_2-$B_{1.0}$	17272.307	8752.8466	5591.05	4052.53	31404.20	0.09615

3. Supported Fig.s

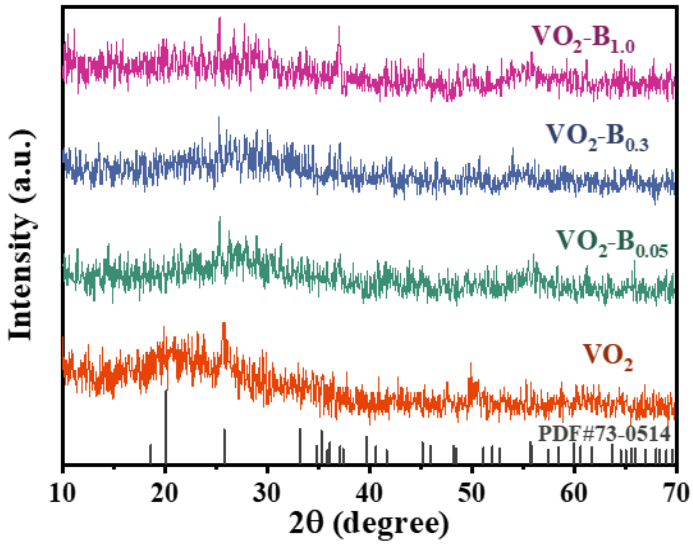

Fig. S1. XRD pattern of VO_2 and VO_2-B_x (x = 0.05, 0.3, 1.0).

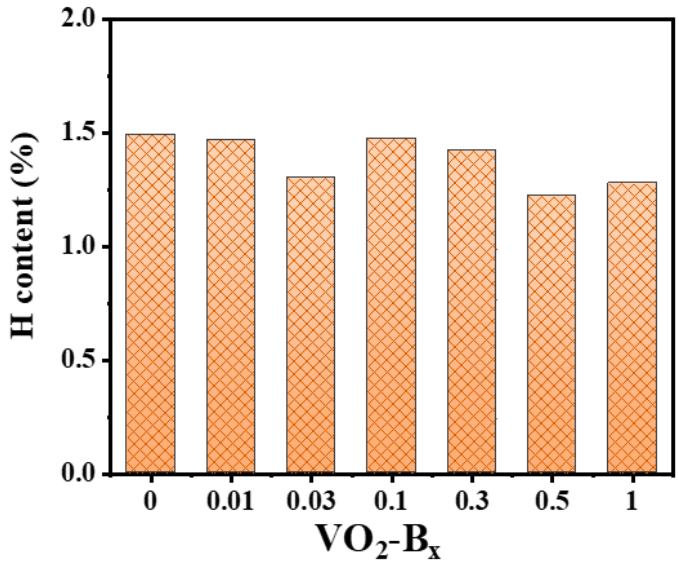

Fig. S2. H content of VO_2 and VO_2-B_x (x = 0.01, 0.03, 0.1, 0.3, 0.5, 1.0).

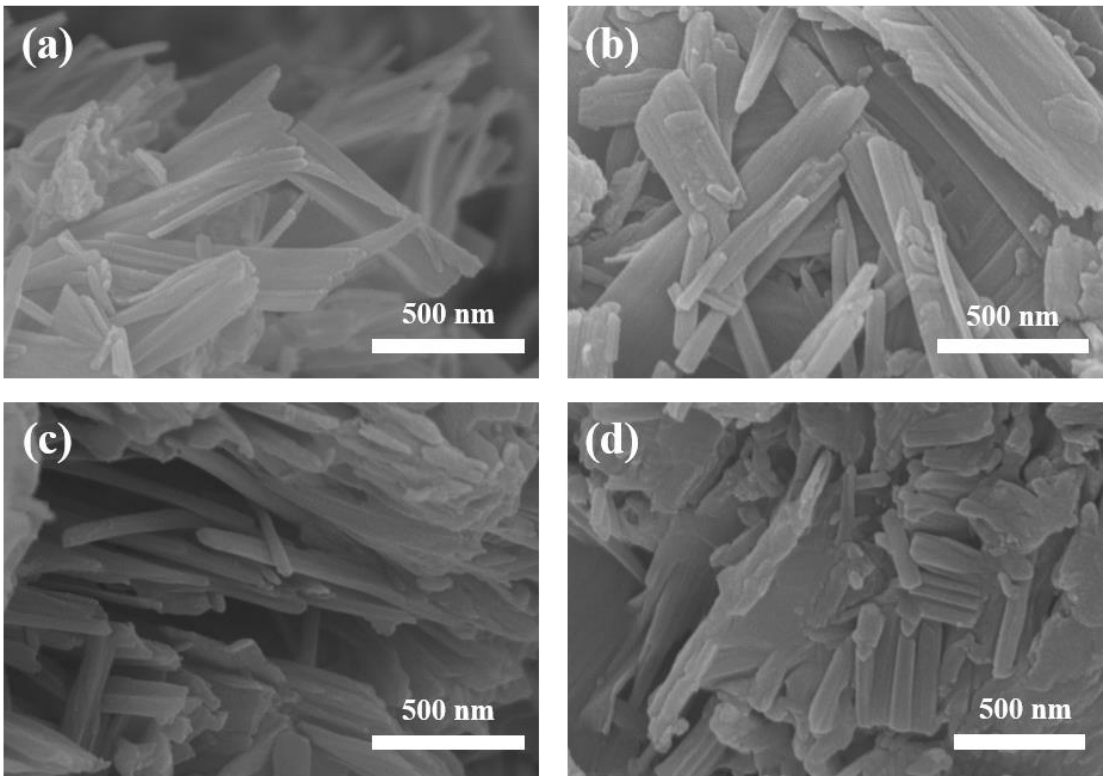

Fig. S3. SEM images of (a) VO_2-$B_{0.05}$, (a) VO_2-$B_{0.1}$, (c) VO_2-$B_{0.3}$, (d) VO_2-$B_{1.0}$.

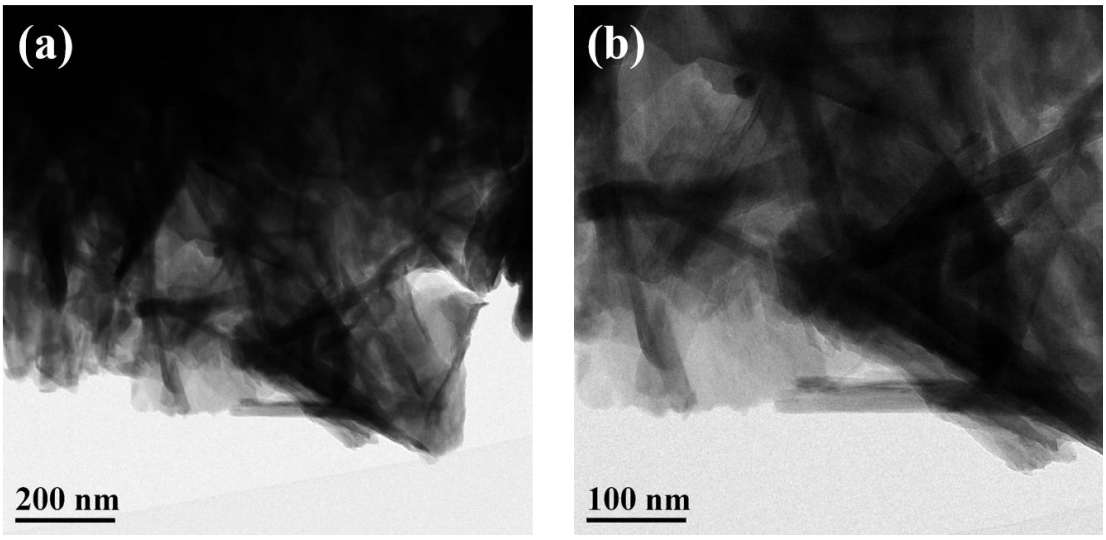

Fig. S4. TEM images of VO_2.

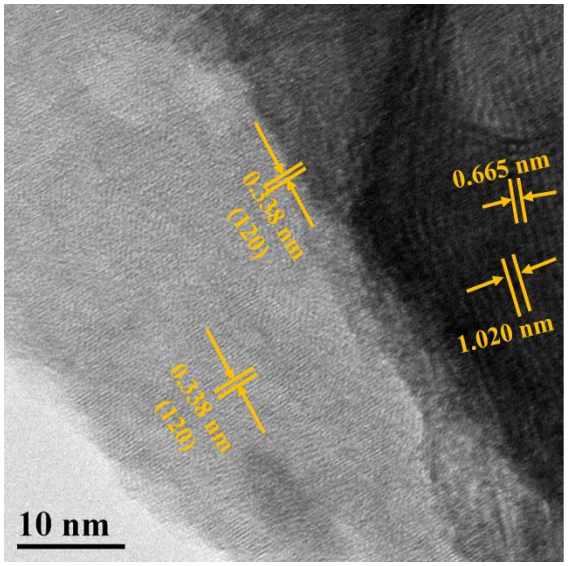

Fig. S5. HR-TEM images of pristine VO_2.

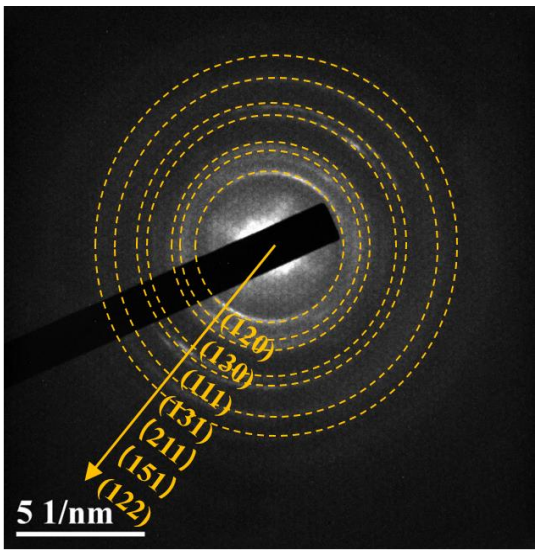

Fig. S6. SAED pattern of VO_2.

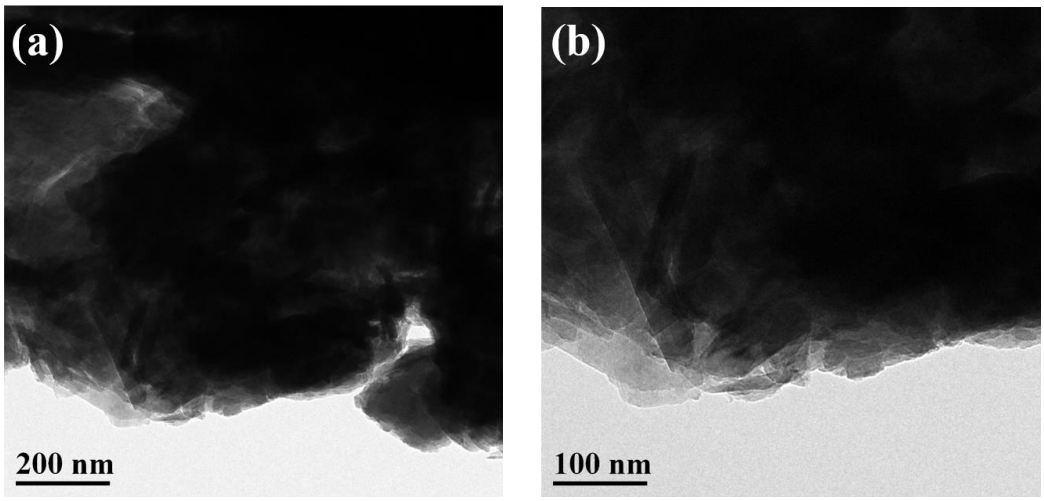

Fig. S7. TEM images of VO_2-$B_{0.5}$.

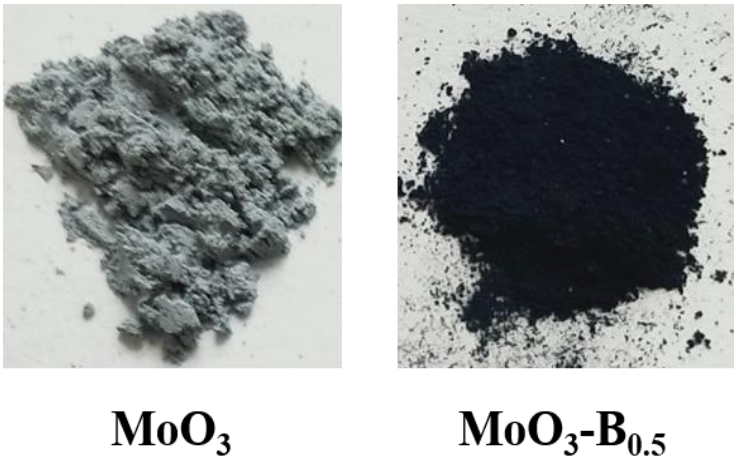

Fig. S8. Photographs of the MoO_3 and MoO_3-$B_{0.5}$ by sodium borohydride grinding treatment.

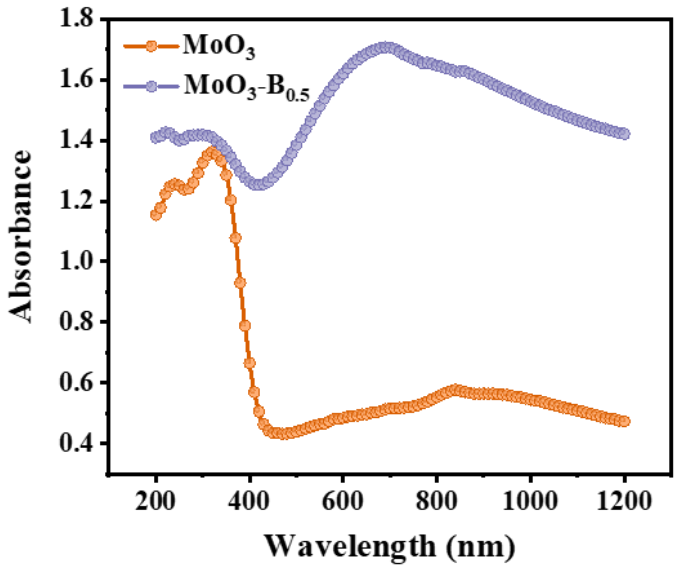

Fig. S9. Ultraviolet-visible diffuse reflectance spectroscopy of MoO_3 and MoO_3-$B_{0.5}$.

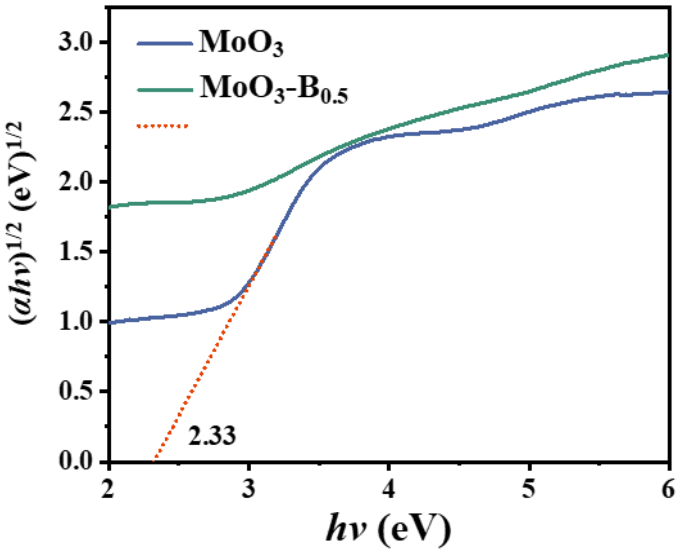

Fig. S10. Tauc's bandgap plot of MoO_3 and MoO_3-$B_{0.5}$.

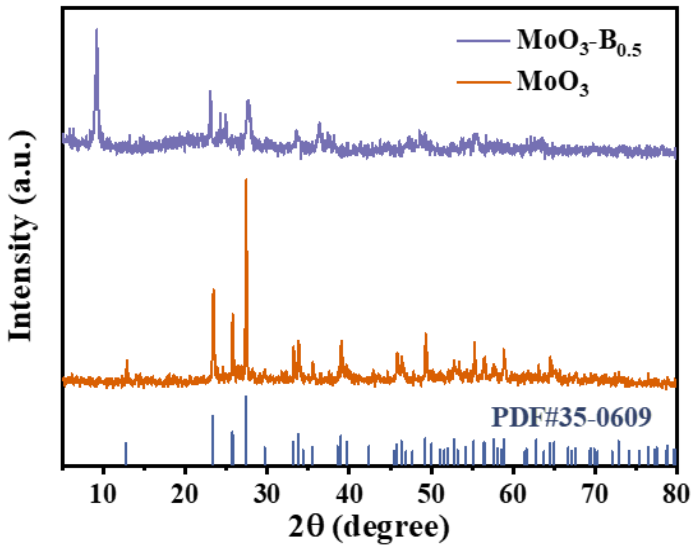

Fig. S11. XRD patterns of MoO_3 and MoO_3-$B_{0.5}$.

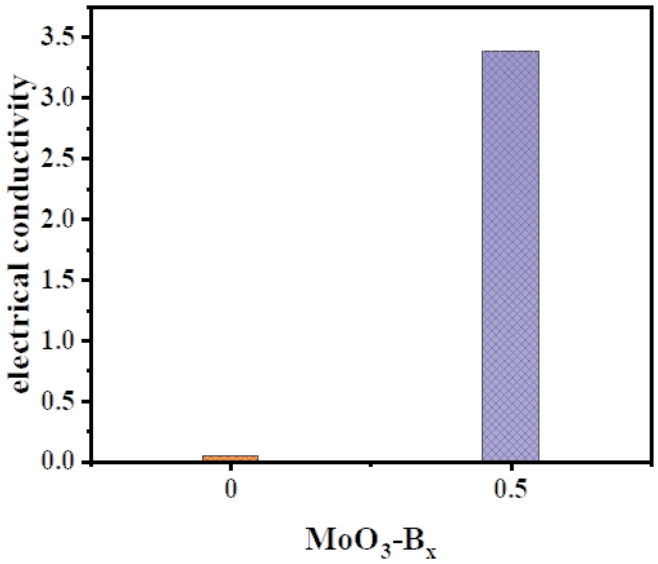

Fig. S12. The electrical conductivity of MoO_3 and MoO_3-$B_{0.5}$.

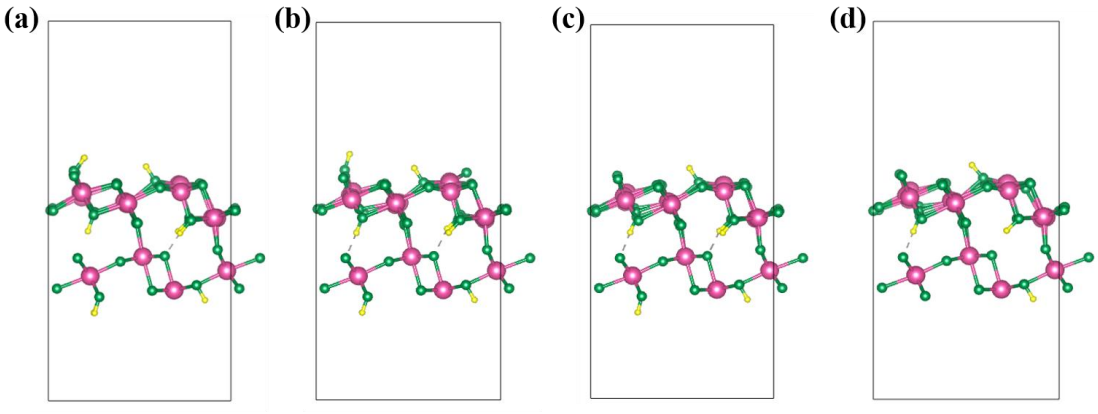

Fig. S13. The front views on the supercells of (a) $H_9V_{32}O_{64}$ (bulk VO_2, 14.0% H-doping), (b) $H_8V_{32}O_{63}$ (1.56% O-vacancy), (c) $H_6V_{32}O_{61}$ (4.69% O-vacancy), (d) $H_4V_{32}O_{59}$ (7.81% O-vacancy). The red balls denote V atoms, the green balls denote O atoms, and the yellow balls means H atoms.

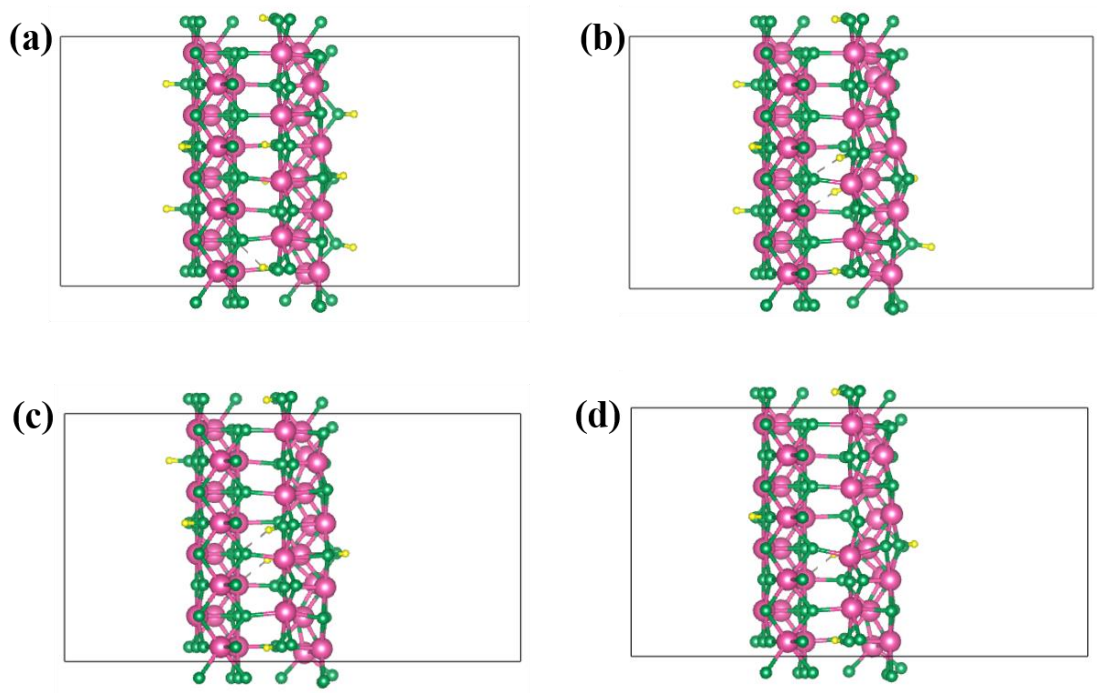

Fig. S14. The profile views on the supercells of (a) $H_9V_{32}O_{64}$ (bulk VO_2, 14.0% H-doping), (b) $H_8V_{32}O_{63}$ (1.56% O-vacancy), (c) $H_6V_{32}O_{61}$ (4.69% O-vacancy), (d) $H_4V_{32}O_{59}$ (7.81% O-vacancy). The red balls denote V atoms, the green balls denote O atoms, and the yellow balls means H atoms.

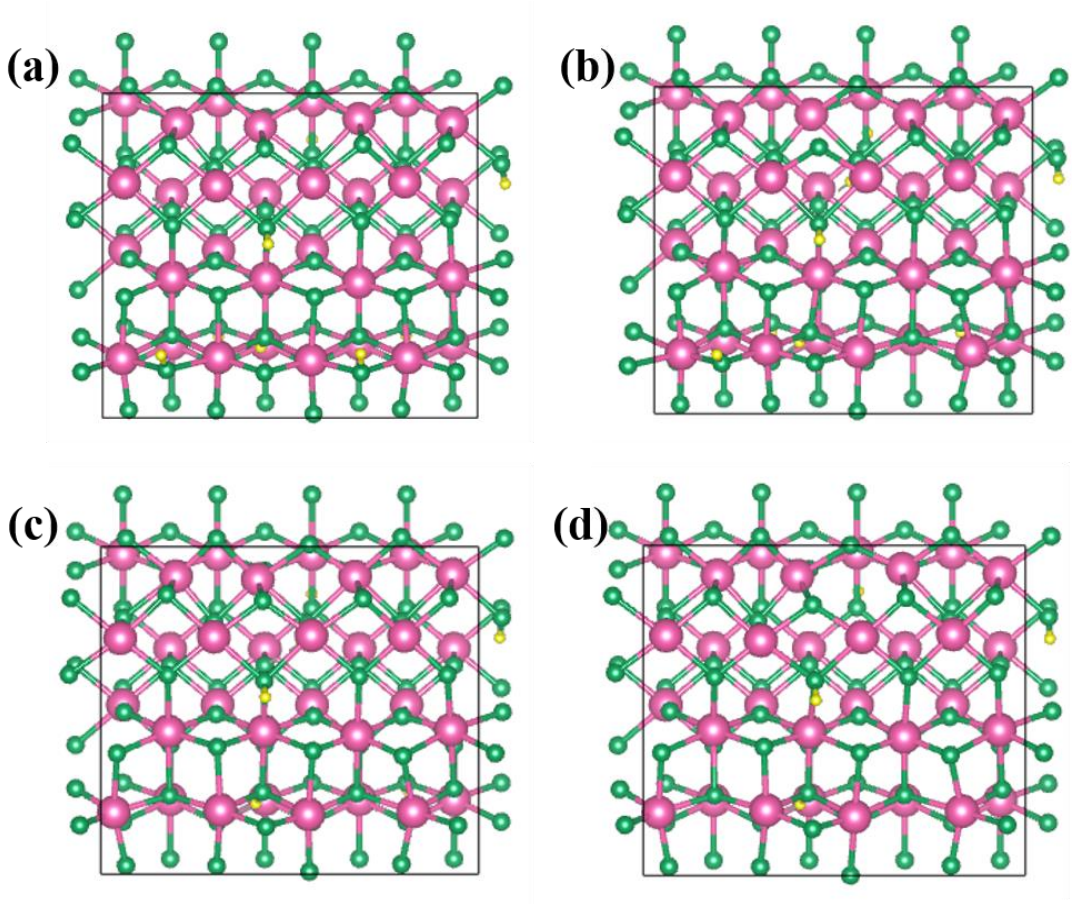

Fig. S15. The aerival views on the supercells of (a) $H_9V_{32}O_{64}$ (bulk VO_2, 14.0% H-doping), (b) $H_8V_{32}O_{63}$ (1.56% O-vacancy), (c) $H_6V_{32}O_{61}$ (4.69% O-vacancy), (d) $H_4V_{32}O_{59}$ (7.81% O-vacancy). The red balls denote V atoms, the green balls denote O atoms, and the yellow balls means H atoms.

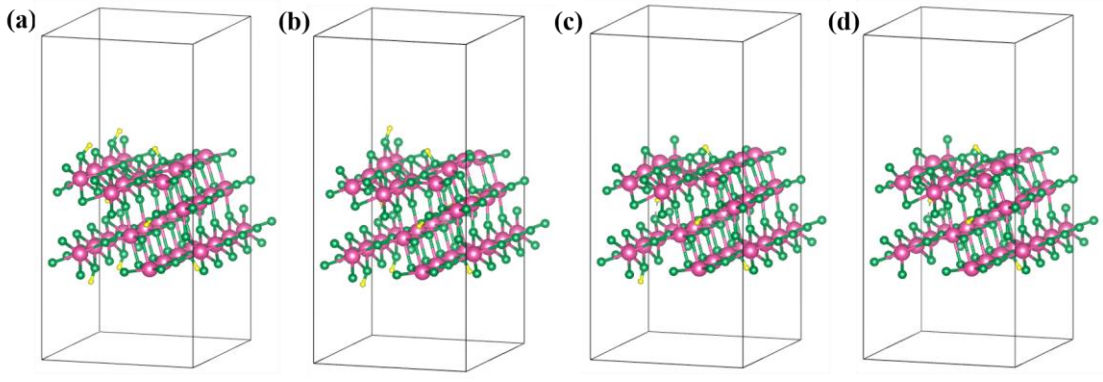

Fig. S16. The stereochemical structures of (a) $H_9V_{32}O_{64}$ (bulk VO_2, 14.0% H-doping), (b) $H_8V_{32}O_{63}$ (1.56% O-vacancy), (c) $H_6V_{32}O_{61}$ (4.69% O-vacancy), (d) $H_4V_{32}O_{59}$ (7.81% O-vacancy). The red balls denote V atoms, the green balls denote O atoms, and the yellow balls means H atoms.

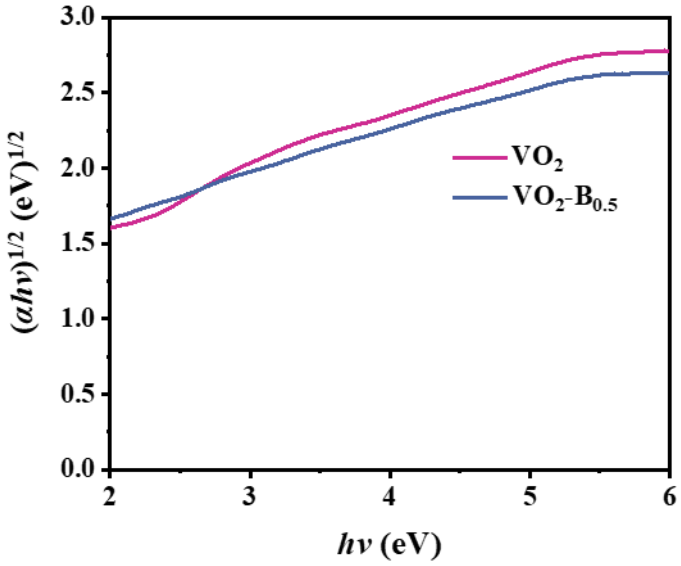

Fig. S17. Tauc's bandgap plot of VO_2 and VO_2-$B_{0.5}$.

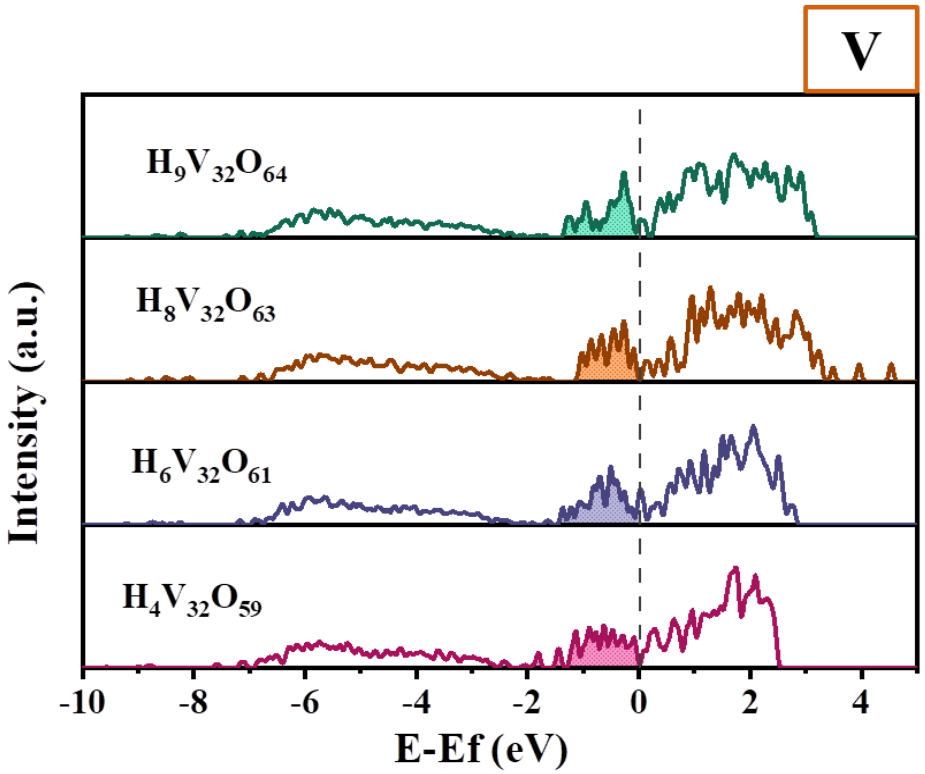

Fig. S18. Simulated density of states (DOS) of V atoms with $H_9V_{32}O_{64}$, $H_8V_{32}O_{63}$, $H_6V_{32}O_{61}$ and $H_4V_{32}O_{59}$ with different content of Oxygen vacancy in the lattice, shaded areas (S1 = 33.47, S2 = 34.63, S3 = 35.44, S4 =37.14).

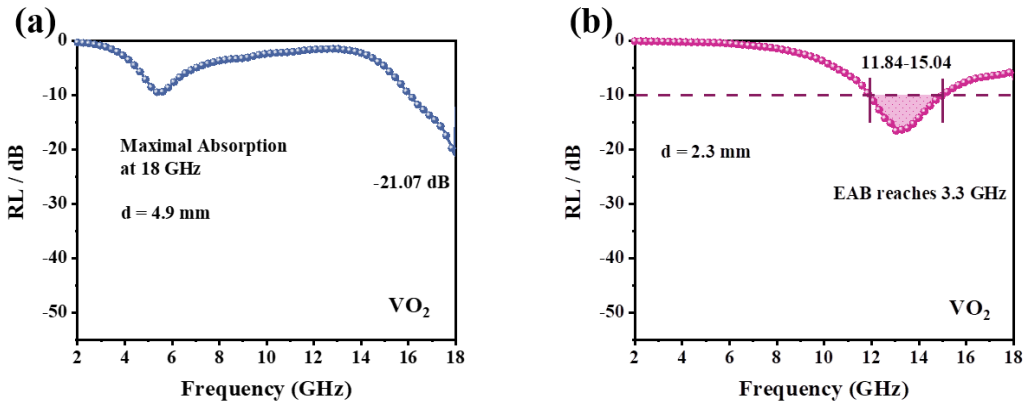

Fig. S19. The reflection loss curves of VO_2 with a sample thickness of (a) 1.9 mm and (b) 2.3 mm.

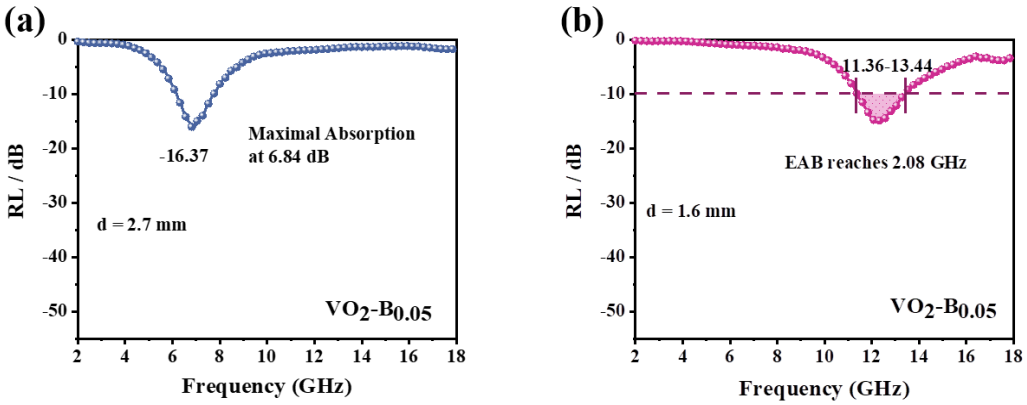

Fig. S20. The reflection loss curves of VO_2-$B_{0.05}$ with a sample thickness of (a) 2.7 mm and (b) 1.6 mm.

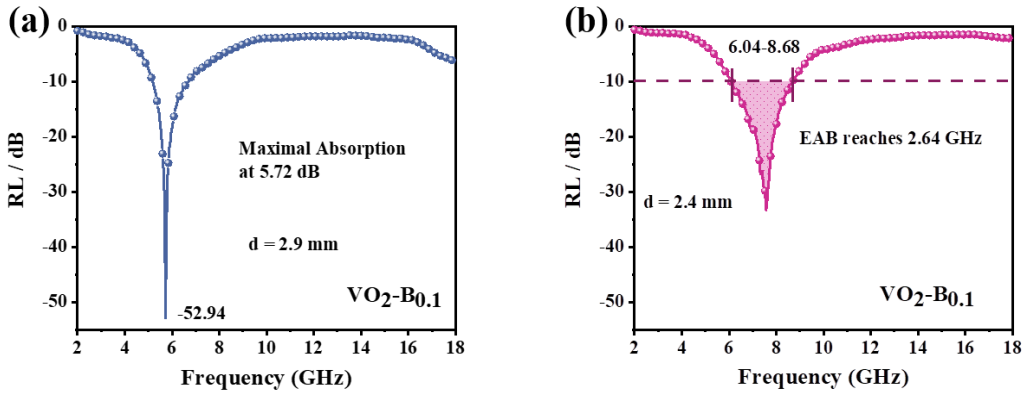

Fig. S21. The reflection loss curves of VO_2-$B_{0.1}$ with a sample thickness of (a) 2.9 mm and (b) 2.4 mm.

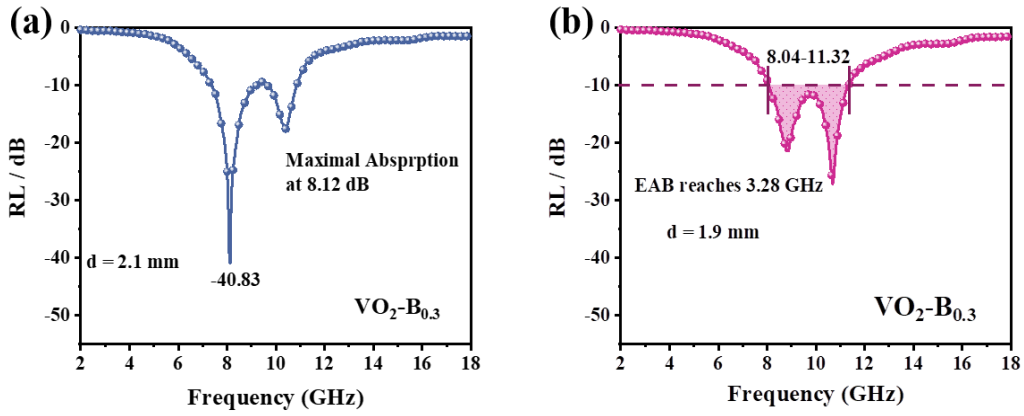

Fig. S22. The reflection loss curves of VO_2-$B_{0.3}$ with a sample thickness of (a) 2.1 mm and (b) 1.9 mm.

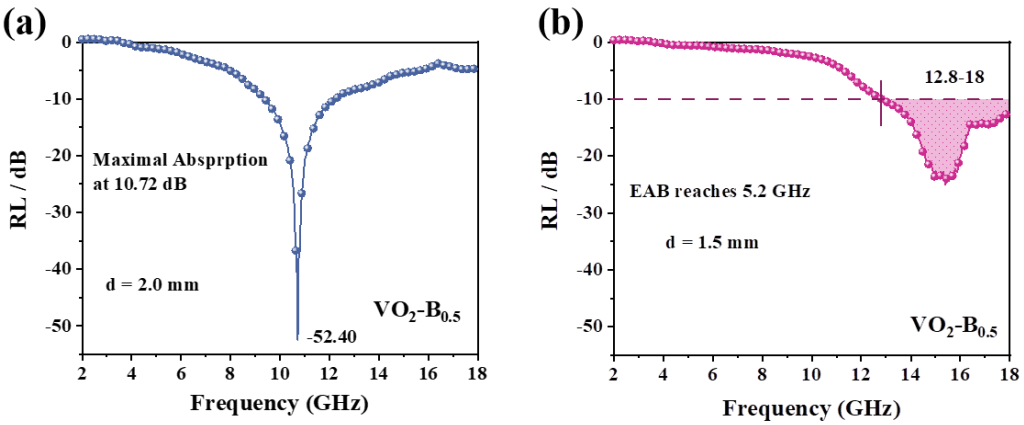

Fig. S23. The reflection loss curves of VO_2-$B_{0.5}$ with a sample thickness of (a) 2.0 mm and (b) 1.5 mm.

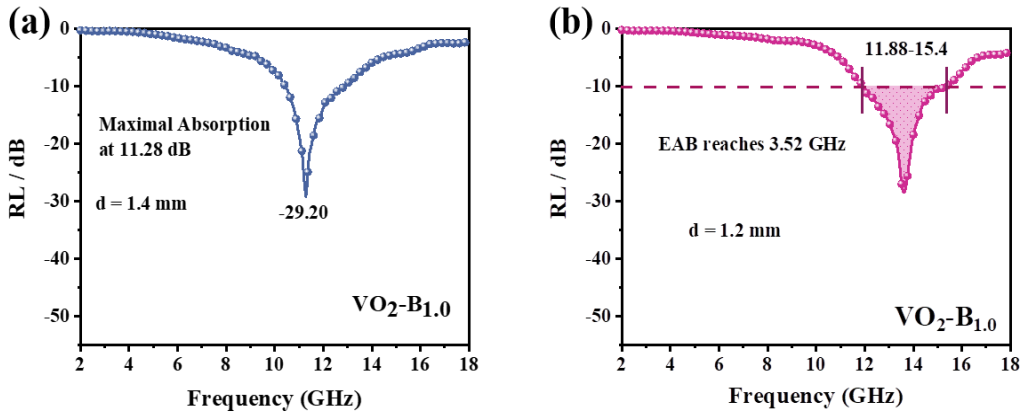

Fig. S24. The reflection loss curves of VO_2-$B_{1.0}$ with a sample thickness of (a) 1.4 mm and (b) 1.2 mm.

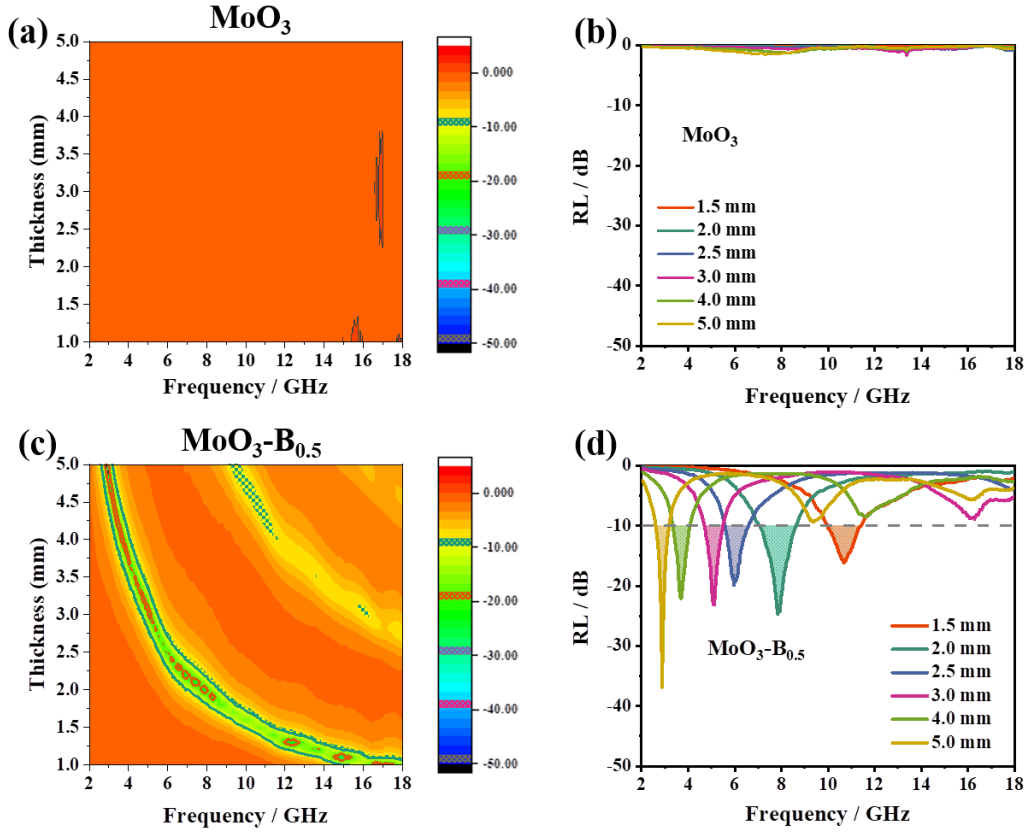

Fig. S25. EMA performance of (a, b) MoO_3, (c, d) MoO_3-$B_{0.5}$.

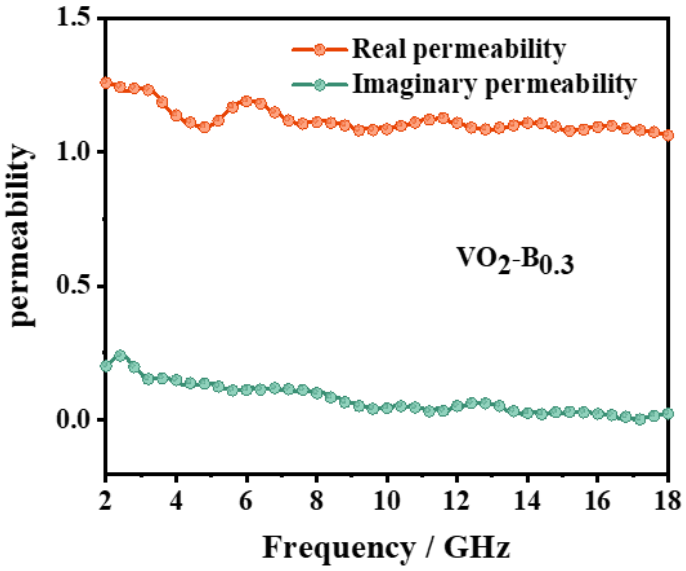

Fig. S26. The real permeability and imaginary permeability of VO_2-B_X.

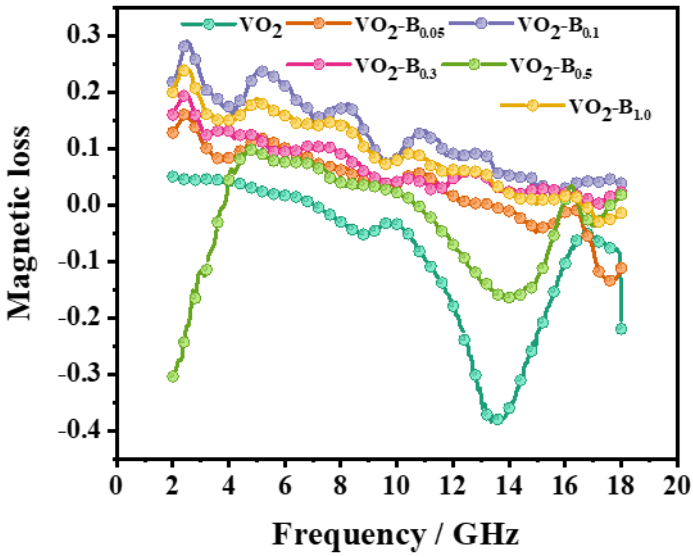

Fig. S27 The magnetic loss of of VO_2 and VO_2-B_x (x= 0.05, 0.1, 0.3, 0.5, 1.0).

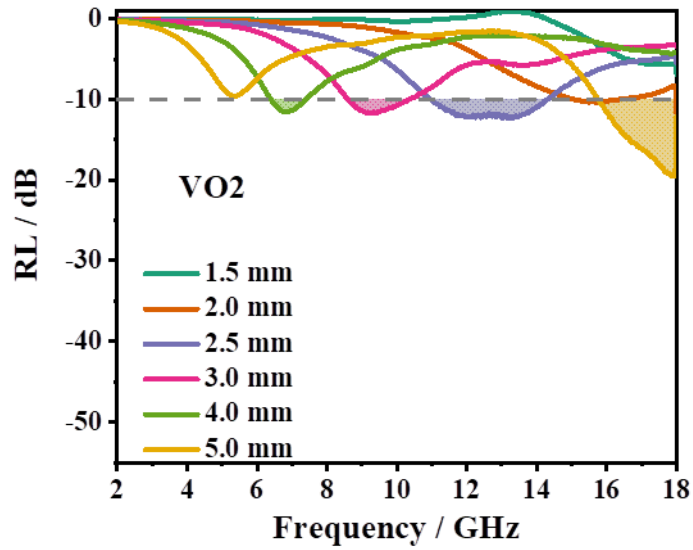

Fig. S28. RL vs. frequency plots of VO_2 (1.5-5.0 mm-thick).

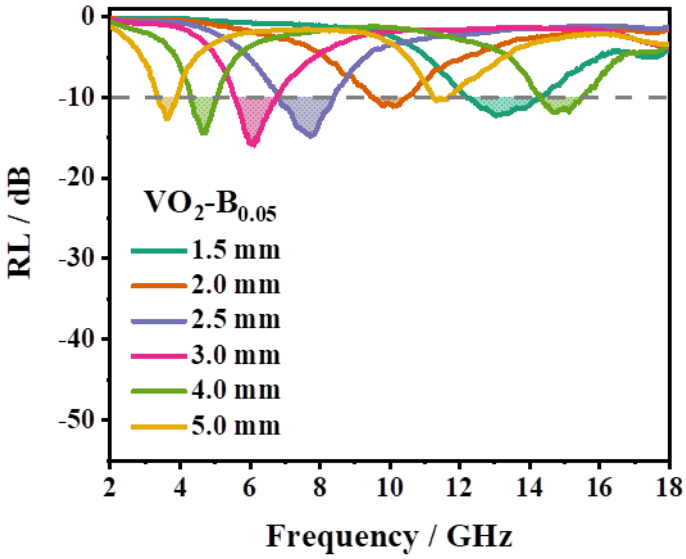

Fig. S29. RL vs. frequency plots of VO_2-$B_{0.05}$ (1.5-5.0 mm-thick).

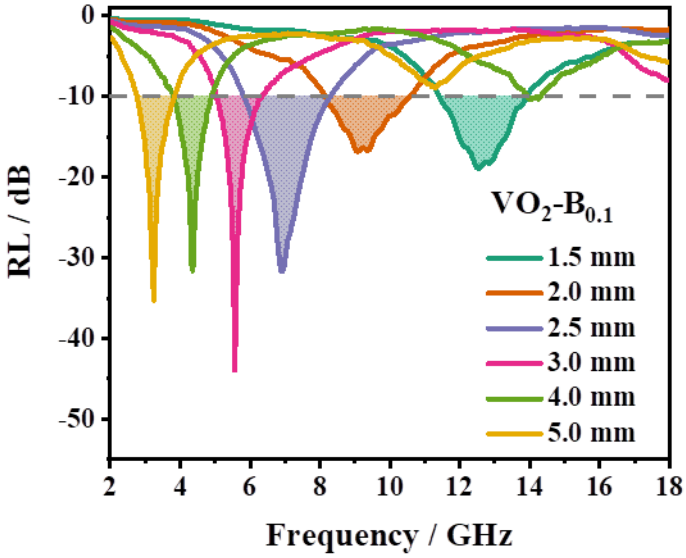

Fig. S30. RL vs. frequency plots of VO_2-$B_{0.1}$ (1.5-5.0 mm-thick).

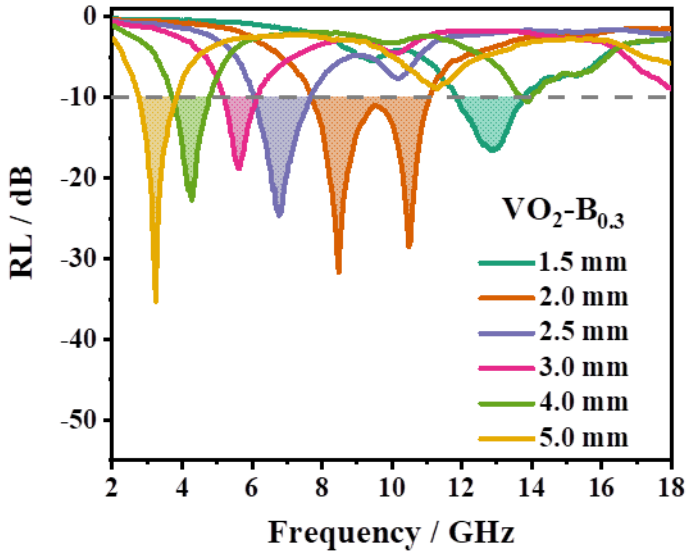

Fig. S31. RL vs. frequency plots of VO_2-$B_{0.3}$ (1.5-5.0 mm-thick).

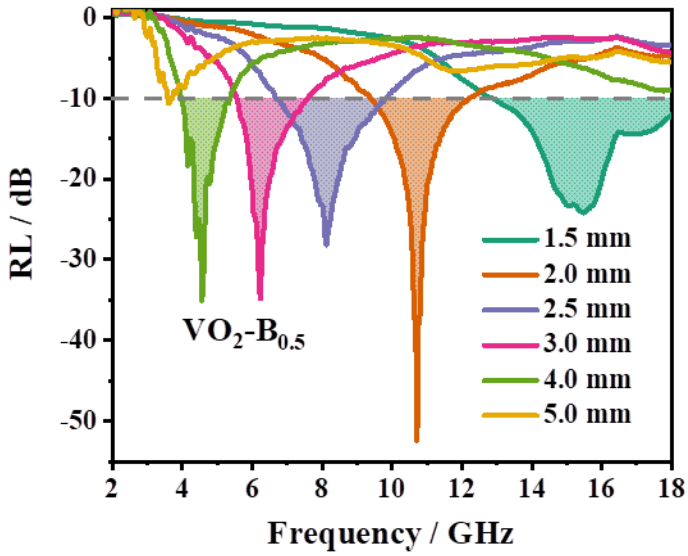

Fig. S32. RL vs. frequency plots of VO_2-$B_{0.5}$ (1.5-5.0 mm-thick).

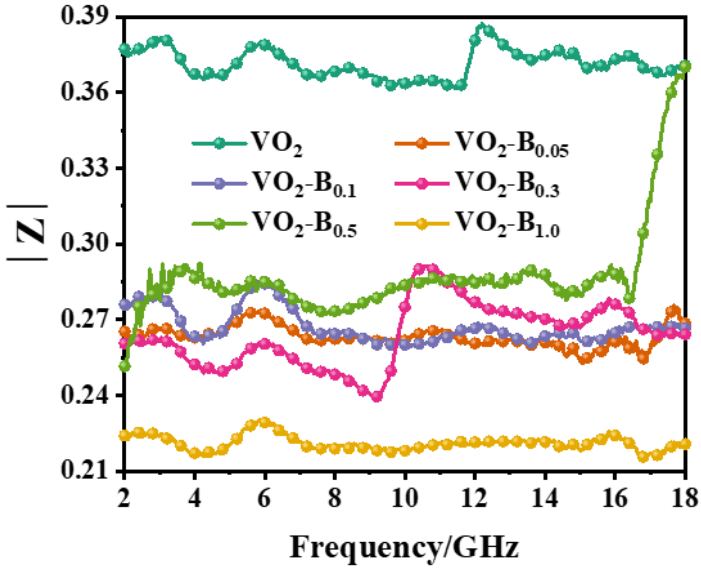

Fig. S33. The impedance values of VO_2-B_x (x= 0.05, 0.1, 0.3, 0.5, 1.0).

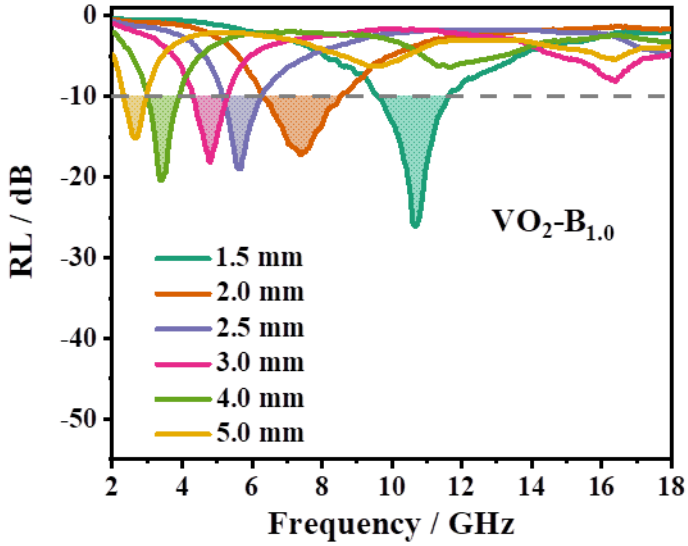

Fig. S34. RL vs. frequency plots of VO_2-$B_{1.0}$ (1.5-5.0 mm-thick).